Manuscript version: Author's Accepted Manuscript
The version presented in WRAP is the author's accepted manuscript and may differ from the published version or Version of Record.

Persistent WRAP URL:
http://wrap.warwick.ac.uk/135090

How to cite:
Please refer to published version for the most recent bibliographic citation information.
If a published version is known of, the repository item page linked to above, will contain details on accessing it.

Copyright and reuse:
The Warwick Research Archive Portal (WRAP) makes this work by researchers of the University of Warwick available open access under the following conditions.

Publisher's statement:
Please refer to the repository item page, publisher's statement section, for further information.

For more information, please contact the WRAP Team at: wrap@warwick.ac.uk.

Microstructural evolution of 316L Austenitic Stainless Steel During In-Situ Biaxial Deformation and Annealing

Authors

Scott Taylor [a] (corresponding author) scott.taylor.1@warwick.ac.uk., Hiren R. Kotadia[a],

[a] WMG, Warwick University, Coventry CV4 7AL, UK.

Abstract

Austenitic stainless steel 316L was investigated by a combination of in-situ biaxial straining and subsequently by in-situ annealing within a Carl Zeiss Sigma FEG-SEM. A Micromecha Proxima stage was used to impart biaxial strain on the sample, results were compared with macro scale testing to validate the method, physical properties were established in close correlation to macro scale tests. Samples were subsequently subjected to annealing cycles using a Gatan Murano 525 heated stage to assess the influence of imparted strain on the recrystallization kinetics of the material. Following annealing trials the material was observed to initiate recrystallization around 100 °C earlier within heavily strained samples at 750 °C in comparison to 850 °C within unstrained samples.

1. Introduction

Austenitic stainless steels have received considerable interest due to their attractive properties and have been extensively exploited as structural materials owing to their high temperature tensile and creep strength and excellent corrosion resistance. Of particular interest in this study, 316L steel offers excellent formability, high strength and excellent corrosion resistance, used extensively within marine, nuclear and biomedical applications [1-3]. During room temperature forming 316L is known to deform due to conventional octahedral slip as a result of low stacking energy and at higher strain rates by twinning deformation which is directly linked to the materials propensity to strain harden [4-5].

The deformation mechanisms, characteristics and strain hardening behaviour of 316L have been investigated widely, with studies looking at macro scale testing and post mortem analysis of microstructures to infer events during deformation [6-7]. The influence of martensitic transformations within the material during straining, and dynamic recrystallization have also been investigated and modelled using macro scale testing [8].

Following deformation energy imparted by strain is stored in point defects and dislocations within a materials microstructure, the increased density of dislocations within the microstructure has a direct influence on the recrystallization of the material during subsequent heating regimes to which it may be exposed [9-10]. During deformation, both SSDs (statistically stored dislocations) and GNDs (geometrically necessary dislocations) are generated but the rate of GND generation is higher leading to an increased density of GNDs; GNDs therefore have a greater influence on work hardening during forming and subsequently on recrystallization kinetics during annealing [11]. To inform the design process correctly an in depth understanding of the recrystallization behaviour of the material in various conditions is required.

There is sometimes a disconnect between academia and industry in terms of the applicability of fundamental studies on microstructural evolution. Industrially, simulation of a process, and macro scale trials are often seen as the quickest way to understanding current problems or assessing new processes. Micro scale testing however can be a powerful tool to help understand the underlying changes in microstructure which impact the macro scale forming and can be used to directly inform material and process design and modification [12].

Post mortem analysis of samples can show what processes have occurred within the materials microstructure but advances in in-situ stages allow for direct observation of microstructural evolution during both deformation and annealing [13-14]. In-situ techniques have been employed to observe the deformation mechanisms of various materials such as aluminium and steel [15-16]; in-situ annealing trials have also been conducted on said materials [17-18]. 316L has been investigated during in-situ tensile testing to observe the twin boundary evolution and crack initiation of the material, but no subsequent annealing treatments were investigated [19].

It should be noted that the effective free surface of a material investigated by in-situ means may have a slight influence on the microstructural evolution. The presence of the free surface allows grains to move across the surface more easily than fully constrained grains within the bulk material; this free surface in turn accommodates movement and rotation of subsurface grains [20]. Studies have shown that this free surface can lead to an increased amount of grain twins across the surface in comparison to the bulk material during in-situ straining [21]. Previous studies have shown that whilst there is some influence on the microstructure; during in-situ annealing tests the surface fraction shows a close correlation to the bulk material in terms of initiation of recrystallization and subsequent grain size and growth [22].

In this study the validity of micro scale physical testing to assess material properties to that of a typical macro scale test was carried out by means of in-situ SEM biaxial tension and ex-situ tensile. In-situ annealing of strained and unstrained samples from in-situ biaxial straining and ex-situ Nakajima testing was then conducted to establish the influence of applied strain on the recrystallization temperature and kinetics of the material. Macro scale samples annealed ex-situ within a furnace were then compared to validate the in-situ tests. The purpose of this testing was firstly to validate the in-situ processes against macro scale tests and secondly to gain a clearly understanding of recrystallization phenomena within the material in various conditions.

2. Material and Methods

Within this study a commercially available 316L austenitic stainless steel was investigated, the composition of which is given in Table 1. The material was nominally supplied in the annealed condition in 0.5 mm sheet and with no further thermomechanical processing applied prior to testing.

Table.1. Composition of 316L tested within this study (wt.%).

Fe	Cr	Ni	Mo	Mn	C	N
Balance	16.0-	10.0-	2.00-	≤2.00	≤0.030	≤0.10
	18.0	14.0	3.00			

Samples were machined by electrical discharge machining to ensure a high quality surface finish in critical regions of the sample and to reduce any potential residual stresses which may be imparted by traditional machining. Sample geometry prior to testing is illustrated in Fig.1a; samples mounted within the SEM are shown in Fig.1b. Following machining samples were mounted to Bakelite discs using melted wax via an established technique and subsequently polished by standard mechanical polishing to a final physical stage using colloidal silica. A final stage consisting of 30 minutes ion beam milling within a Hitachi IM4000 was employed to ensure a high quality surface finish.

Samples of nominal 0.5 mm thickness were tested within a Micromecha Proxima stage with biaxial grips pre-titled to 70° to allow EBSD (Electron back scattered diffraction) scans to be conducted in-situ. A 3kN load cell and built in digital extensometers with an accuracy of ±0.25% samples were used to control tests. Tests were using cross head speed control with a constant speed of 0.1um/s and paused for EBSD scans which were conducted with load still applied. Following sample failure sections were taken from near the failure region which experienced maximum strain and from the shoulder section within the grips which experienced no strain during testing.

These samples were then mounted in a Gatan Murano 525 heated stage pre-titled to 70° stage and subjected to heat treatments similar to that detailed in Fig.1c and d. Samples were heated at 10 Cs^{-1} and held for two minutes at the desired temperature then returned to 200°C which took around two minutes, EBSD scans were conducted at 200°C where the microstructure was stable and no issues with thermal drift were observed. EBSD scans for both biaxial and annealing samples were conducted sing a 240µm aperture operating at 20keV with an average 1µm step size, scans took approximately two minutes per region. Existing features across the samples surface were used to ensure the same region was observed throughout all scans, no extra fiducial markers were added.
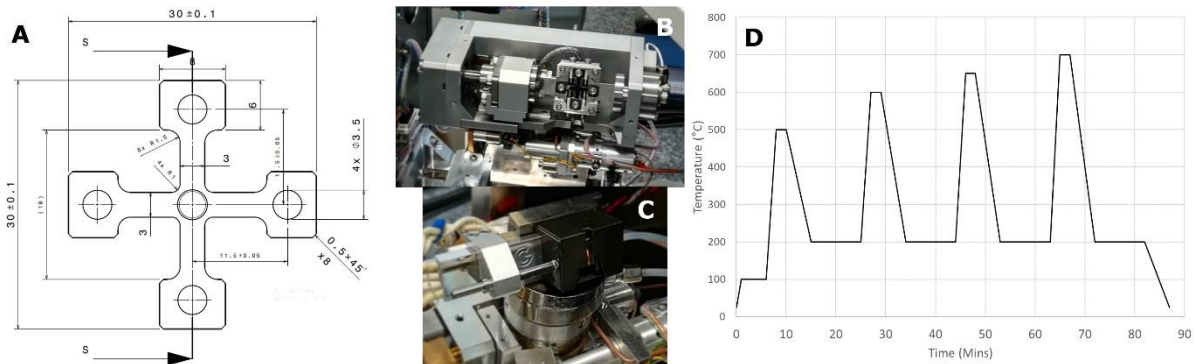

Fig.1. a) Biaxial sample geometry, b) biaxial sample within micromecha Proxima stage mounted within SEM, c) Gatan Murano heated stage mounted within SEM, d) example heating cycle to establish recrystallization temperature.

Macro scale tensile samples were CNC machined and then tested using an Instron 5567 load frame with physical extensometers, Bluehill software was used to control the tests operating in cross head speed control. Tests were carried out to ISO:6892 standard [23]. Macro samples for annealing trials were prepared from forming limit curve samples with 0.5 mm thickness and a 100 mm width which were formed using an ITC Interlaken 1000 kN hydraulic press operating a Nakajima punch and smooth clamp ring set. Tests were run at a constant punch speed of 1 mm/s^{-1}. Full details of the test programme are detailed in previous studies [24]. Samples were tested to failure and sections then taken from regions which had experienced levels of equivalent strain; detailed in eqn.1 of the same magnitude as those within in-situ straining tests.

3. Results and Discussions

3.1. Initial Microstructure

EBSD scans were conducted on the material prior to testing to understand the microstructure in the as received condition. Shown in Fig.2.b. a fine equiaxed structure with an average grain size of 9 µm was observed, two large grains are highlighted which were used as reference points for microstructural observations. Initial GND density within the sample the map of which is shown in fig.2.c was 0.1 x^{14}/m^2 as expected from an annealed sample having undergone full stress relief, and indicating that there was no strain imparted onto the material surface during sample preparation. GND

densities were calculated using Channel 5 software and a KAM (kernel average misorientation) with a filter size of 5x5 and a subgrain angle of 5° [25].

3.2. In-situ biaxial deformation

Stress and strain values were logged throughout testing using Poros 2 software, the resultant curve is illustrated in fig.2a. 0.2% proof stress of the material was calculated using the line intercept method [23] as 301 MPa which is in close agreement with macro scale tensile testing conducted internally and in agreement with the suppliers datasheet [26,27]. As reported elsewhere 316l steel follows the Hall-Petch relationship for grain size and yield strength, as such the value can vary significantly so validation against the materials supplied datasheet is important to establish the suitability of the technique [28] This result shows the validity of the test to establish material properties whilst investigating microstructural evolution directly. Reductions in stress and the jaggedness of the curve were caused by stress relief whilst the crosshead was paused to allow for EBSD. Scans which were conducted at 200 μm increments to observe changes in the microstructure during deformation.

Fig.2d shows the IPF (inverse pole figure) map of the same region as fig.2.b following deformation near to the failure region, the same two grains are highlighted in both images. Following deformation there is a clear increase in size of the grains as well as changes in IPF colouring indicating changes within the orientation of the microstructure. The corresponding GND map is shown in fig.2e which shows a significant increase in GND with an average density of $4.8 \times 10^{14}/m^2$, build ups of dislocations were observed along strain bands within grains as highlighted. Dislocation density is closely linked to material recrystallization, the effect of this increased density was the investigated for its impact on the recrystallization temperature [29].
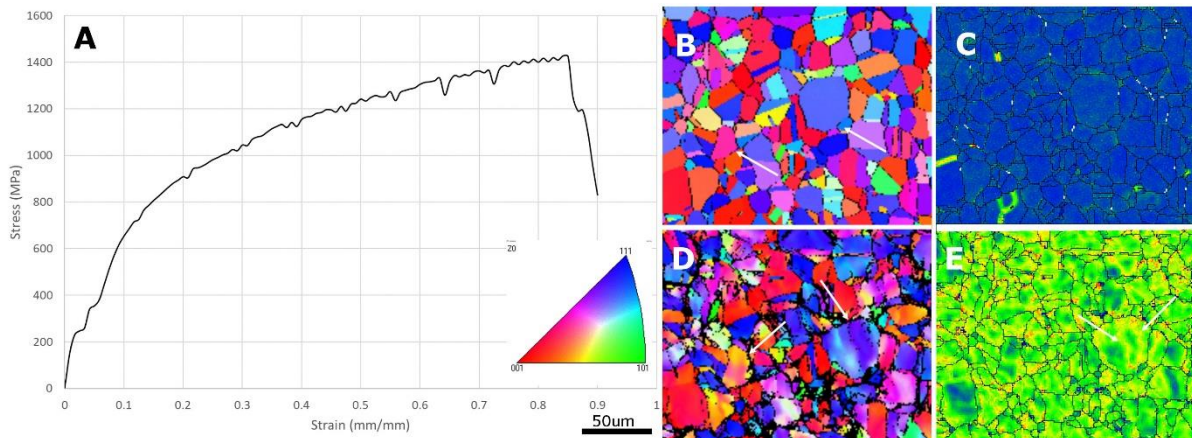

Fig.2. a) Stress strain curve of 316L derived from biaxial testing, b) initial IPF map of 316L prior to test, c) initial GND density map prior to test, d) IPF map near to failure region following test, e) GND density map near to failure following testing.

3.3. In-situ annealing

Within regions of interest for recrystallization kinetics; equivalent strain which is based on localised thinning of the material, where T_o is original thickness and T_s is strained thickness; was calculated using eqn. 1. Two regions; one from the shoulder area of the sample which had experienced zero strain during testing and one from near to the failure region which had experienced around 50% equivalent strain were subjected to increasing annealing temperatures until recrystallization was evident.

$$\left(\left(\frac{To}{Ts}\right) - 1\right) x\ 100$$

Equation 1. Equivalent strain

Fig.3a and b illustrate the IPF map and GND map for the unstrained sample prior to annealing, with an average dislocation density of $0.25 \times 10^{14}/m^2$. This value is higher than reported earlier and was likely due to some residual stresses from sample preparation for in-situ annealing which requires removal of samples from Bakelite discs. The sample was heated in 50°C increments showing no evidence of recrystallization or recovery until 850°C as shown in the IPF map in fig 3c where a fully recrystallized structure with no evidence of parent grains was observed. A reduction of GND density to $0.1 \times 10^{14}/m^2$ was also observed in fig 3d. confirming recrystallization of the sample.
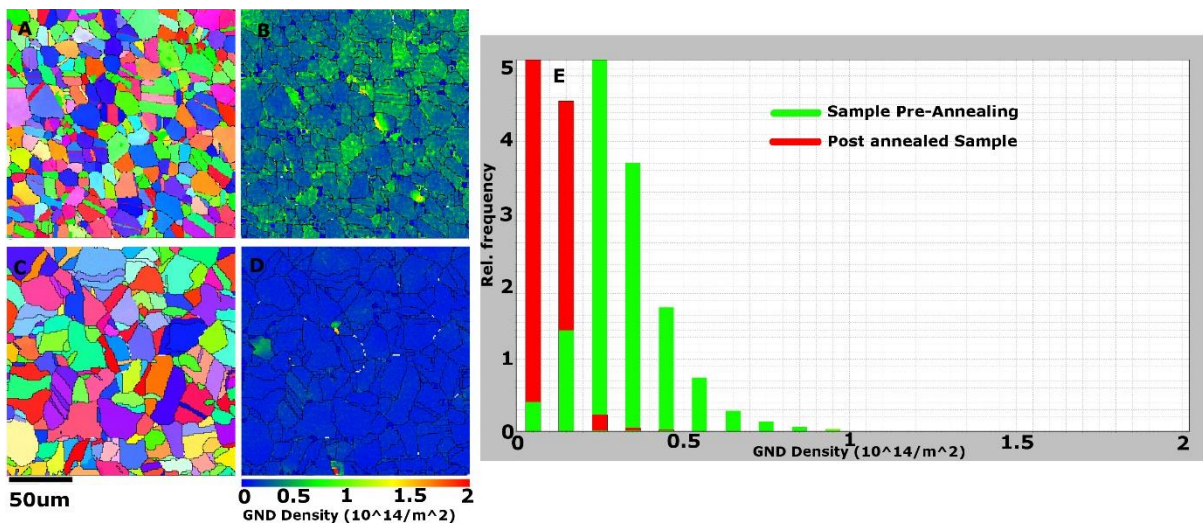

Fig.3. a) IPF map of 316L within shoulder region having experienced no strain pre annealing, b) GND density map of same region pre annealing, c) IPF map of the same region following annealing at 850C, d) GND density map following annealing, e) histogram of GND densities pre and post annealing.

Corresponding IPF and GND maps for the strained sample are shown in fig.4a and d, a more deformed microstructure with elongated grains is seen in the IPF map when compared to the non-strained region. Average GND density across the sample was $2.5 \times 10^{14}/m^2$ due to increased stored energy from strain imparted during testing. As with the unstrained sample 50°C increments were employed until any evidence of microstructural evolution was observed. At 700°C there was an observed reduction of average GND to $0.85 \times 10^{14}/m^2$ but no evidence of recrystallization within the IPF figure shown in fig. 4b indicating recovery of the microstructure at this temperature. An increase in temperature to 750°C lead to a reduction in GND density to $0.1 \times 10^{14}/m^2$ as shown in fig.4f and a recrystallized grain structure with no evidence of parent grains as shown in fig.4c.
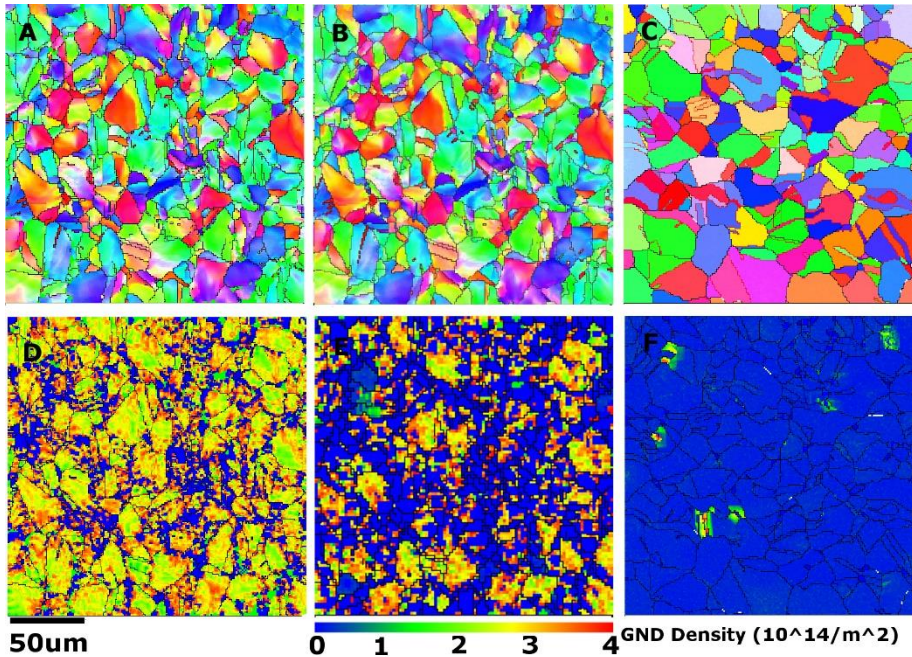
Fig.4. a) IPF map of strained region prior to annealing, b) IPF map of region after heating to 700°C, c) IPF map of region after heating to 750°C, d) GND density map of strained region prior to annealing, e) GND density map of region after heating to 700°C, f) GND density map of region after heating to 750°C,

This reduction in recrystallization temperature is directly related to the level of stored energy imparted during deformation which is stored as GNDs within the microstructure [10]. Subsequent heating then leads to a restructuring of the microstructure; which, within the strained sample has a greater driving force due to increased levels of stored energy and hence recrystallizes at a lower temperature when compared to the unstrained material [9]. The initiation of recrystallization at this temperature is in agreement with results from studies elsewhere which helps validate this technique for understanding the microstructural evolution in-situ [30,31].

3.4. Ex-situ annealing of macro samples

Ex-situ macro scale samples for annealing were formed within an Interlaken press using a Nakajima hemispherical tool, to give a sample size more representative of industrial processes. Following forming regions of the material that had experienced around 50% equivalent strain were sectioned and then exposed to various annealing temperatures within a furnace to establish the recrystallization behaviour of the material. Samples had a thermocouple attached and were then placed into the furnace which was already at temperature, allowed to reach temperature, held for two minutes and then removed and air quenched. Several samples were used to observe the microstructure at differing temperatures but GND values were obtained within each region prior to heating to ensure the same levels of stored energy.
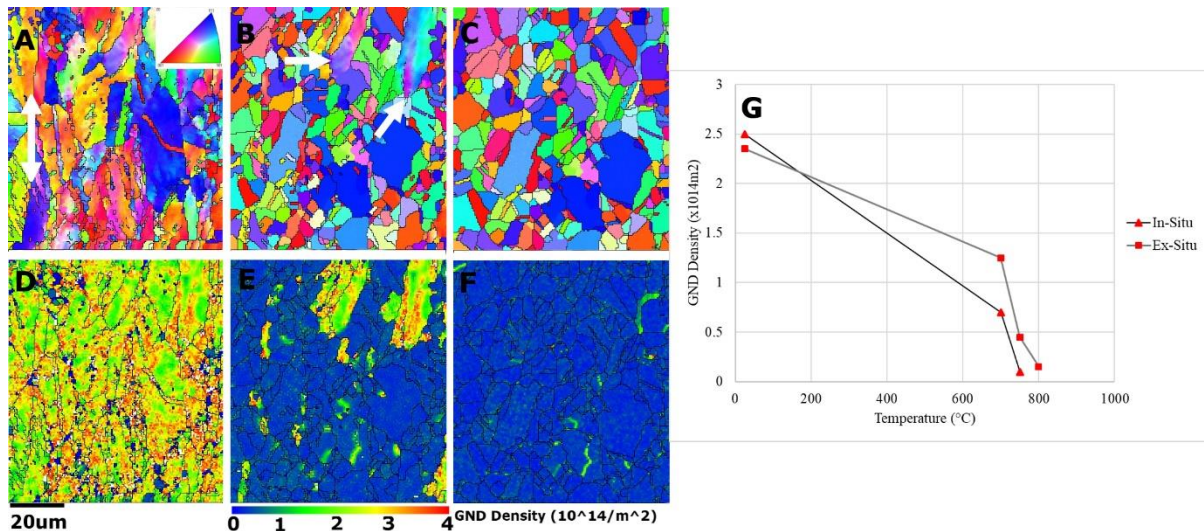
Fig.5. IPF maps of 316L a) following Nakajima testing, b) following heating to 750°C showing partial recrystallization, c) following heating to 800°C showing a fully recrystallized structure, d) GND density map of strained region following testing, e) GND density map of region after heating to 750°C, f) GND density map of region after heating to 800°C g) reduction in GND density for both materials at various temperatures.

Fig.5a shows the microstructure of the material post forming, partial elongation of grains in the direction of deformation is evident. Deformation direction is more evident as deformation was not purely biaxial as within in-situ samples. GND density shown in fig.5.d of the material was established as $2.35 \times 10^{14}/m^2$ which is close to that of the in-situ samples confirming that as well as the same reduction in thickness both materials have similar levels of stored energy within the GNDs. Within fig.5b following heating to 750°C the material appears to be heavily recrystallized but not completely; with non-recrystallized grains highlighted. These partially recrystallized grains are observed in fig.5.e as regions of higher GND density than the surrounding recrystallized microstructure. Fig.5.c then shows the sample following heating to 800°C where we observe full recrystallization, fig.5.f shows the GND density as $0.15 \times 10^{14}/m^2$ indicating a fully recrystallized structure.

These results show the close correlation between ex-situ forming and annealing and in-situ versions of the same process, demonstrating that the results from in-situ experiments can be used to directly influence and inform the industrial design process. The microscale in-situ results showing slightly increased recrystallization kinetics due to the presence of the upper free surface allowing for easier accommodation of movement and rotation of grains within the microstructure.

3.5. Free surface influence

With the presence of the free surface within in-situ samples compared to the fully constrained microstructure within the bulk material microstructural evolution could be impacted due to the easier movement and accommodation of new grains within the in-situ samples [32]. Table.2 captures various physical properties from both in-situ and ex-situ annealing trials. Initial GND values are near identical with samples taken from regions having experienced around 50% equivalent strain so having the same levels of stored energy. Grain sizes were established using Channel 5 software and were within close agreement, the slightly larger initial grain size within the ex-situ samples being due to the uniaxial imparted deformation rather than biaxial. Following annealing GND densities for both materials were around $0.1 \times 10^{14}/m^2$ as expected from fully annealed strain free materials.

Table.2. Physical properties of material following in-situ and ex-situ tests

	Initial Grain Size (µm)	Std. Dev.	Initial GND Density ($10^{14}/m^2$)	Std. Dev.	Annealed Grain Size (µm)	Std. Dev.	Annealed GND Density ($10^{14}/m^2$)	Std. Dev.	Recrystallization Initiation (°C)
In-Situ	13.4	5.4	2.15	1.8	12.1	4.9	0.1	0.2	750
Ex-Situ	13	4.8	2.35	2.0	7.7	3.2	0.15	0.3	750

Recovery and recrystallization initiated at the same temperature within both samples, however full recrystallization was not observed until 800°C within the ex-situ samples compared to 750°C within the in-situ samples, illustrated in fig.5.d. Indicating that the free surface has some influence on the recrystallization kinetics but that the initiation temperature is independent of this, depending rather on levels of stored energy [33]. Within the in-situ samples the dominant mechanism is likely recovery followed by limited recrystallization, whereas within the ex-situ samples we observe less evidence of recovery and instead partial recrystallization. This difference in mechanisms in combination with the increased freedom of motion would help explain the increased grain size within ex-situ samples with more energy available for recrystallization and grain growth than within the in-situ samples. Following annealing grain sizes as given in table 2 were observed to be around 60% larger within the in-situ material at 12.1µm compared to 7.7µm; which is in close agreement with results reported elsewhere and is due to the mobility of the grains on the surface rather than the constrained microstructure slowing grain growth [34.35].

4. Conclusions

From this study we draw four main conclusions, the first being the validity of the biaxial test set up and methodology when compared to that of a macro scale test to establish material properties. This validation means that direct observations of microstructural evolution can be directly related to strain within macro scale forming to help inform the understanding of the materials deformation characteristics and inform industrial design.

Secondly we observe that 316L under heavily strained conditions will undergo recovery at 700°C and recrystallize at the lower temperature of 750°C compared to a temperature of 850°C in the unstrained condition.

Thirdly we conclude that the in-situ annealing experimental work is in close agreement with ex-situ macro scale investigations, verifying the process and also confirming its validity within an industrial context.

Finally we conclude that the influence of the free surface within in-situ testing will have an influence on the final microstructure, being responsible for around a 60% increase in average grain size. This free surface has little to no influence on the initiation of recrystallization temperature of the material which is more dependent on the levels of stored energy within the material.

Data Availability

The raw/processed data required to reproduce these findings cannot be shared at this time due to technical or time limitations.

References

1. Lee, W. S., Chen, T. H., Lin, C. F., & Luo, W. Z. (2011). Dynamic mechanical response of biomedical 316L stainless steel as function of strain rate and temperature. Bioinorganic Chemistry and Applications, 2011. https://doi.org/10.1155/2011/173782

2. Kruml, T., Polák, J., & Degallaix, S. (2000). Microstructure in 316LN stainless steel fatigued at low temperature. Materials Science and Engineering A, 293(1–2), 275–280. https://doi.org/10.1016/S0921-5093(00)01015-7

3. Gerland, M., Alain, R., Ait Saadi, B., & Mendez, J. (1997). Low cycle fatigue behaviour in vacuum of a 316L-type austenitic stainless steel between 20 and 600°C - Part II: Dislocation structure evolution and correlation with cyclic behaviour. Materials Science and Engineering A, 229(1–2), 68–86. https://doi.org/10.1016/s0921-5093(96)10560-8

4. Hong, S. G., & Lee, S. B. (2004). The tensile and low-cycle fatigue behavior of cold worked 316L stainless steel: Influence of dynamic strain aging. International Journal of Fatigue, 26(8), 899–910. https://doi.org/10.1016/j.ijfatigue.2003.12.002

5. Wang, S., Wei, K., Li, J., Liu, Y., Huang, Z., Mao, Q., & Li, Y. (2019). Enhanced tensile properties of 316L stainless steel processed by a novel ultrasonic resonance plastic deformation technique. Materials Letters, 236, 342–345. https://doi.org/10.1016/j.matlet.2018.10.080

6. Leo, J. R. O., Pirfo Barroso, S., Fitzpatrick, M. E., Wang, M., & Zhou, Z. (2019). Microstructure, tensile and creep properties of an austenitic ODS 316L steel. Materials Science and Engineering A, 749, 158–165. https://doi.org/10.1016/j.msea.2019.02.014

7. Sinha, S., Szpunar, J. A., Kiran Kumar, N. A. P., & Gurao, N. P. (2015). Tensile deformation of 316L austenitic stainless steel using in-situ electron backscatter diffraction and crystal plasticity simulations. Materials Science and Engineering A, 637, 48–55. https://doi.org/10.1016/j.msea.2015.04.005

8. Man, J., Obrtlík, K., Petrenec, M., Beran, P., Smaga, M., Weidner, A., Dluhoš, J., Kruml, T., Biermann, H., Eifler, D., & Polák, J. (2011). Stability of austenitic 316L steel against martensite formation during cyclic straining. Procedia Engineering, 10, 1279–1284. https://doi.org/10.1016/j.proeng.2011.04.213

9. Humphreys, F. J., & Hatherly, M. (2004). The Structure and Energy of Grain Boundaries. In Recrystallization and Related Annealing Phenomena (pp. 91–119). Elsevier. https://doi.org/10.1016/b978-008044164-1/50008-6

10. Raabe, D. (2014). Recovery and Recrystallization: Phenomena, Physics, Models, Simulation. In Physical Metallurgy: Fifth Edition (Vol. 1, pp. 2291–2397). Elsevier Inc. https://doi.org/10.1016/B978-0-444-53770-6.00023-X

11. Jiang, J., Britton, T. B., & Wilkinson, A. J. (2013). Evolution of dislocation density distributions in copper during tensile deformation. Acta Materialia, 61(19), 7227–7239. https://doi.org/10.1016/j.actamat.2013.08.027

12. Taylor, S., Masters, I., Li, Z., & Kotadia, H. R. (2019). Direct Observation via In Situ Heated Stage EBSD Analysis of Recrystallization of Phosphorous Deoxidised Copper in Unstrained and Strained Conditions. Metals and Materials International. https://doi.org/10.1007/s12540-019-00493-y

13. Zhang, S., Zeng, W., Zhao, Q., Ge, L., & Zhang, M. (2017). In situ SEM study of tensile deformation of a near-β titanium alloy. Materials Science and Engineering A, 708, 574–581. https://doi.org/10.1016/j.msea.2017.10.028

14. Gussev, M. N., & Leonard, K. J. (2019). In situ SEM-EBSD analysis of plastic deformation mechanisms in neutron-irradiated austenitic steel. Journal of Nuclear Materials, 517, 45–56. https://doi.org/10.1016/j.jnucmat.2019.01.034

15. Caër, C., & Pesci, R. (2017). Local behavior of an AISI 304 stainless steel submitted to in situ biaxial loading in SEM. Materials Science and Engineering A, 690, 44–51. https://doi.org/10.1016/j.msea.2017.02.087

16. Zhang, J. Z., He, X. D., Tang, H., & Du, S. Y. (2008). Direct high resolution in situ SEM observations of small fatigue crack opening profiles in the ultra-fine grain aluminium alloy. Materials Science and Engineering A, 485(1–2), 115–118. https://doi.org/10.1016/j.msea.2007.08.006

17. Thomas, I., Zaefferer, S., Friedel, F., & Raabe, D. (2003). High-Resolution EBSD Investigation of Deformed and Partially Recrystallized IF Steel. Advanced Engineering Materials, 5(8), 566–570. https://doi.org/10.1002/adem.200300373

18. Kapoor, I., Lan, Y., Rijkenberg, A., Li, Z., & Janik, V. (2018). Quasi in-situ analysis of geometrically necessary dislocation density in α-fibre and γ-fibre during static recrystallization in cold-rolled low-carbon Ti-V bearing microalloyed steel. Materials Characterization, 145, 686–696. https://doi.org/10.1016/j.matchar.2018.09.032

19. Wang, W., Liu, T., Cao, X., Lu, Y., & Shoji, T. (2017). In-situ observation on twin boundary evolution and crack initiation behavior during tensile test on 316L austenitic stainless steel. Materials Characterization, 132, 169–174. https://doi.org/10.1016/j.matchar.2017.08.020

20. Clark, S., Janik, V., Rijkenberg, A., & Sridhar, S. (2016). Analysis of the extent of interphase precipitation in V-HSLA steels through in-situ characterization of the γ/α transformation. Materials Characterization, 115, 83–89. https://doi.org/10.1016/j.matchar.2016.03.021

21. Jin, Y., Lin, B., Bernacki, M., Rohrer, G. S., Rollett, A. D., & Bozzolo, N. (2014). Annealing twin development during recrystallization and grain growth in pure nickel. Materials Science and Engineering A, 597, 295–303. https://doi.org/10.1016/j.msea.2014.01.018

22. KERISIT, C., LOGÉ, R. E., JACOMET, S., LLORCA, V., & BOZZOLO, N. (2013). EBSD coupled to SEM in situ annealing for assessing recrystallization and grain growth mechanisms in pure tantalum. Journal of Microscopy, 250(3), 189–199. https://doi.org/10.1111/jmi.12034

23. BS EN ISO 6892-1:2019 Metallic materials. Tensile testing. Method of test at room temperature, British Standards International, 2019.

24. Taylor, S., Masters, I., Li, Z., & Kotadia, H. R. (2019). Influence of Elevated Temperatures on Mechanical Properties and Microstructure of C106 Copper Investigated by In Situ Heated Stage EBSD Analysis. Metallurgical and Materials Transactions A: Physical Metallurgy and Materials Science, 50(10), 4493–4497. https://doi.org/10.1007/s11661-019-05374-y

25. Konijnenberg, P.J., Zaefferer, S., Raabe, D., (2015). Assessment of Geometrically Necessary Dislocation Levels Derived by 3D EBSD. Acta Materialia, 99, 402-414. http://dx.doi.org/10.1016/j.actamat.2015.06.051

26. Taylor, S., Masters, I., Li, Z., & Kotadia, H. R. (2019). Comparison of Formability and Microstructural Evolution of C106 Copper and 316L Stainless Steel. JOM, 71(8), 2721–2727. https://doi.org/10.1007/s11837-019-03603-8

27. Forta 316L/4404EN 1.4404, ASTM TYPE 316L / UNS S31603 Datasheet from steelfinder.outukump.com, https://secure.outokumpu.com/steelfinder/GradeDataSheetv3PDF.aspx?OKGrade=4404&Category=Forta, Accessed 07.01.20

28. Qin, W., Li, J., Liu, Y., Kang, J., Zhu, L., Shu, D., Peng, P., She, D., Meng, D., & Li, Y. (2019). Effects of grain size on tensile property and fracture morphology of 316L stainless steel. Materials Letters, 254, 116–119. https://doi.org/10.1016/j.matlet.2019.07.058

29. Hutchinson, W. B. (1984). Development and control of annealing textures in low-carbon steels. International Metals Reviews, 29(1), 25–40. https://doi.org/10.1179/imtr.1984.29.1.25

30. Li, J., Cao, Y., Gao, B., Li, Y., & Zhu, Y. (2018). Superior strength and ductility of 316L stainless steel with heterogeneous lamella structure. Journal of Materials Science, 53(14), 10442–10456. https://doi.org/10.1007/s10853-018-2322-4

31. Li, J., Mao, Q., Nie, J., Huang, Z., Wang, S., & Li, Y. (2019). Impact property of high-strength 316L stainless steel with heterostructures. Materials Science and Engineering A, 754, 457–460. https://doi.org/10.1016/j.msea.2019.03.105

32. Konijnenberg, P. J., Zaefferer, S., & Raabe, D. (2015). Assessment of geometrically necessary dislocation levels derived by 3D EBSD. Acta Materialia, 99, 402–414. https://doi.org/10.1016/j.actamat.2015.06.051

33. Nowell, M. M., Field, D. P., Wright, S. I., & Lillo, T. M. (2004). In-situ EBSD investigation of recrystallization in ECAE processed copper. Materials Science Forum, 467–470(II), 1401–1406. https://doi.org/10.4028/www.scientific.net/msf.467-470.1401

34. Brisset, F., Helbert, A. L., & Baudin, T. (2013). In situ electron backscatter diffraction investigation of recrystallization in a copper wire. Microscopy and Microanalysis, 19(4), 969–977. https://doi.org/10.1017/S1431927613000299

35. Nakamichi, H., Humphreys, F. J., & Brough, I. (2008). Recrystallization phenomena in an IF steel observed by in situ EBSD experiments. Journal of Microscopy, 230(3), 464–471. https://doi.org/10.1111/j.1365-2818.2008.02006.x